AIAA JOURNAL
Vol. 43, No. 2, February 2005

Experimental Investigation of a Pulse Detonation Engine with a Two-Dimensional Ejector

Daniel Allgood* and Ephraim Gutmark†
University of Cincinnati, Cincinnati, Ohio 45221
and
Adam Rasheed‡ and Anthony J. Dean‡
General Electric Global Research Center, Niskayuna, New York 12309

A parametric study into the integration of a pulse detonation engine (PDE) with an ejector was performed. High-speed shadowgraph visualizations of the flow inside the two-dimensional ejector provided a qualitative method of determining the performance of the integrated system. The performance was observed to be sensitive to the inlet geometry of the ejector as well as its axial position relative to the exhaust plane of the PDE. Significant levels of entrainment were obtained when the ejector's inlet was contoured, whereas flow separation reduced entrainment efficiency in the ejector with a straight thin inlet lip. Also, the high-speed shadowgraph visualizations showed that the entrainment produced by the PDE–ejector system could be modified by the presence of an exhaust nozzle on the PDE. Qualitative analysis of the high-speed images using the coherent structure velocimetry method was conducted to obtain pseudovelocity information.

Introduction

PULSE detonation engines (PDEs) are currently being investigated as a new technology for aerospace propulsion. One of the main advantages of PDEs is that detonations create less entropy when they combust a fuel/oxidizer mixture than conventional constant-pressure processes such as those used in current gas turbines. Because of the inherently unsteady nature of PDEs, one of the main challenges to making practical engines is minimizing the losses at the inlet and outlet.

Ejectors are fluid pumps that are used to entrain secondary flows using a primary flow. For propulsion applications, this entrainment can augment thrust compared to that generated by the primary flow alone and thereby increase performance. The use of steady-flow ejectors and their associated design procedures is well established. The application of ejectors, however, to unsteady primary flows is less common. Several studies[1–3] have examined unsteady ejectors driven by pulse jets or other devices by which the primary airflow was unsteady. Some of the results by Porter and Squyers[1] reported thrust augmentation using a pulse-jet driver by as much as a factor of 1.8. The theoretical augmentation limit for a steady-isentropic-flow ejector of similar geometry was shown to have a value of 1.6. The results indicated that unsteady ejectors are dominated by flow mechanisms different from those seen in steady ejectors. The enhanced performance of unsteady ejectors is typically associated with a more efficient energy transfer process between the primary flow and the secondary (entrained) flow through inviscid processes, whereas the steady ejector relies primarily on viscous shear mixing. In fact, some analytical studies have indicated that the best performance for unsteady ejectors can be attained for relatively short ejector lengths with a fluid pulse that is of high momentum, low mass, and short duration.[4] These results suggest that ejectors could be highly effective in increasing the performance of PDEs.

Preliminary experimental studies of 152.4-mm-diam ejectors driven by 50.8-mm-diam PDEs at 20 and 40 Hz measured entrained mass flows to be a factor of 2 greater than the primary flow,[5] but no thrust measurements were reported. These experiments also indicated that, under certain conditions, strong backflows upstream could be induced for a portion of the cycle. Another series of experiments using a 50-mm-diam H_2/air PDE tube at 10 Hz with 76.2-, 101.6-, and 152.4-mm-diam ejectors showed that the thrust augmentation varied significantly with the axial position of the ejector relative to the PDE tube exit.[6] Thrust augmentation levels varied from +16 to −5% depending on the configuration. In all cases, the maximum thrust augmentation was found to occur with the ejector located fully downstream of the PDE tube. Numerical simulations of the aforementioned configuration showed significant mass entrainment for the high-thrust-augmentation configurations. Similar experiments using C_2H_4/air showed maximum thrust augmentation levels of 24%, depending on the configuration, and additionally captured flow visualization shadowgraph images at the ejector inlet throughout one cycle.[7] In both of the preceding studies, the experimentally measured thrust augmentation was significantly lower than the factor of 1.8 achieved by Porter and Squyers's pulse-jet experiments.

Computational studies of single-shot PDE-driven straight ejectors using an Euler code demonstrated the importance of the ejector-to-PDE tube diameter ratio in achieving thrust augmentation and its sensitivity to fill fraction.[8] Multiple cycle simulations of a specific converging/diverging ejector at approximately 120 Hz using an Euler code with finite rate chemistry showed thrust augmentation of almost 80% (Ref. 9). Further nondetonation computational studies highlighted the importance of the starting vortices, precursor shocks, and direct pressure loads created by the gas-dynamic (shock-tube) processes within the ejector to the overall thrust-augmentation performance of the system.[10] These computations suggested that high thrust augmentation for PDE–ejector applications is achievable and highlighted the need to understand the gasdynamics, resonance phenomena, and flow interactions of the PDE–ejector system for optimum performance.

One reason for the discrepancy in thrust augmentation in the referenced works could be due to differences in the shape of the ejector inlet. The inlet shape is an aerodynamic surface that will have a significant impact on how the secondary flow will be entrained. For the referenced detonation-driven ejector studies,[5,7–9] the ejector

Presented as Paper 2004-0864 at the 42nd Aerospace Sciences Meeting, Reno, NV, 5–8 January 2004; received 6 February 2004; revision received 18 August 2004; accepted for publication 19 August 2004.

*Research Assistant, Department of Aerospace Engineering and Engineering Mechanics. Student Member AIAA.
†Ohio Eminent Scholar, Professor, Department of Aerospace Engineering and Engineering Mechanics, 746 Baldwin Hall; Ephraim.Gutmark@uc.edu.
‡Research Engineer, Energy and Propulsion Technologies Laboratory.

inlets did not have a smooth radius contour. Only the experiments in Ref. 6 had ejector inlets that were contoured.

In the present investigation, high-speed shadowgraph visualizations of the flow inside a two-dimensional ejector provided a qualitative method of determining the performance of the system. Sensitivity to the ejector inlet geometry as well as the ejector's axial position relative to the exhaust plane of the PDE were observed and recorded. Analysis of the high-speed images using the coherent structure velocimetry (CSV) technique[11] of tracking flow features was also conducted, providing pseudovelocity information. In addition to providing insight into PDE–ejector flow physics, these data will be valuable for calibrating computational fluid dynamics codes and ultimately for the optimization of PDE–ejector configurations for propulsion applications.

Experimental Facility

The parametric visualization study into the integration of a PDE with an ejector was performed using the PDE test facility at General Electric Global Research. The PDE tube had a total nominal length of 1.04 m (L_{PDE}). It consisted of two sections: the first section was a 0.66-m-long, 50.8-mm-diam pipe that contained a series of orifice plates to enhance the deflagration-to-detonation transition (DDT) process. This section was followed by a 0.38-m-long, 50.8×50.8 mm^2 square-cross-section tube (3-mm wall thickness). The square section was mounted at the end of the round tube to provide a means for testing the two-dimensional nozzles and ejectors. The ejector walls were constructed of 25.4-mm-thick optical-grade cast acrylic sheets, allowing optical access to the internal flow as shown in Fig. 1. The top and bottom walls of the ejectors and nozzle were interchanged to study various geometries. The ejector was 0.20 m long for all tests, and the walls were spaced 152.4 mm apart to give an ejector-to-PDE area ratio of 3.0. Air supplied from facility compressors flowed continuously into the tube through two opposing holes at the head end, and the hydrogen fuel was pulsed via a solenoid valve to obtain nominally stoichiometric conditions. Fuel and air were mixed directly in the tube using a mixing element and were ignited by a spark plug mounted one diameter downstream of the fuel/air mixing element. The airflow rate was maintained at 0.068 kg/s and the tube was fired at low frequency to protect the acrylic sidewalls. The PDE cycle frequency and fill fraction were kept constant at values of 10 Hz and 1.0, respectively.

A high-speed shadowgraph imaging system was used to visualize the flow at the exit of the PDE tube and within the ejector. The system consisted of a continuous light source (Oriel 200-W xenon mercury arc lamp), 304.8-mm spherical mirrors (focal length 1.90 m), and a high-framing-rate digital camera (Vision Research Phantom 7) arranged in a modified Z configuration. To avoid saturation of the image from both the light source and flame luminosity, neutral density filters were used to attenuate the light before entering the camera. The camera was pretriggered off the spark signal of the PDE. The framing rate was 27,000 frames/s with each frame being exposed for 1 μs, during which time the detonation wave would move approximately 2 mm within the image. This resulted in smearing of the initial exiting detonation wave in the images but provided excellent clarity during the majority of the PDE cycle.

Time-accurate gauge pressure measurements inside the PDE were obtained using fast-response dynamic pressure transducers (PCB model 113A20) and were correlated with the high-speed shadowgraph imaging. The dynamic pressure transducers had a resolution of 0.725mV/kPa and resonant frequency of greater than 500 kHz. The pressure data were sampled at 500 kHz using a National Instruments

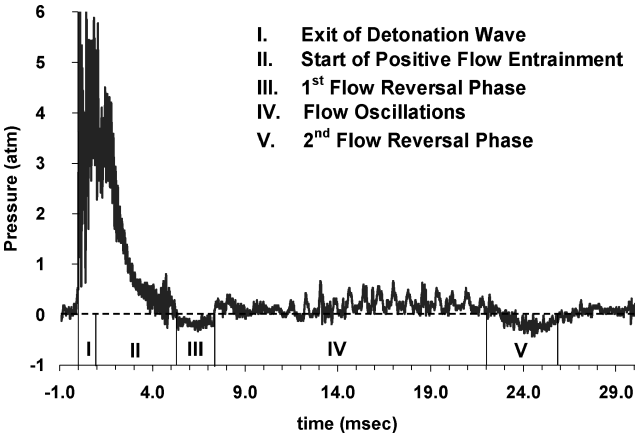

Fig. 2 Sample gauge pressure time trace and phases of the PDE–ejector cycle.

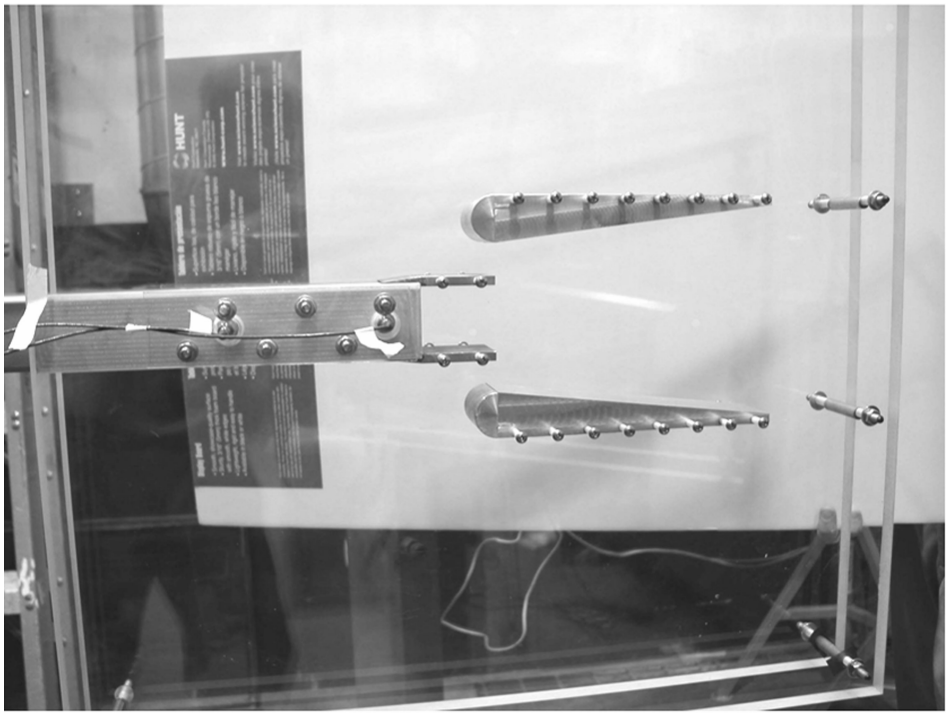

Fig. 1 Two-dimensional PDE–ejector with optical access.

data acquisition board. One pressure transducer was located at the headwall of the PDE ($x/L_{\mathrm{PDE}} = 0$), and two transducers were located near the exit of the PDE at axial locations of x/L_{PDE} equal to 0.88 and 0.98. The two transducers located near the end of the PDE were used to measure the wave speed and verify detonation. Measured wave velocities were 2030 ± 100 m/s, which are comparable to the Chapman–Jouguet detonation velocity for stoichiometric H_2/air of 1980 m/s.

A series of two-dimensional PDE ejectors and nozzles was designed and built at the University of Cincinnati and tested using the high-speed shadowgraph system. The axial placement of the ejector relative to the PDE exhaust nozzle could be adjusted in 25-mm increments in both the downstream and upstream directions. The test matrix reported in this paper is given in Table 1. The shadowgraph visualizations for this test matrix were performed with the PDE operating at a cycle frequency of 10 Hz. Because of the temperature

Table 1 PDE–ejector test matrix

Ejector internal geometry	Ejector inlet geometry	PDE exit nozzle geometry[a]	Ejector axial position
Straight	No contour	Straight (AR = 1.0)	Inline
Diverging	Round contour	Diverging	Upstream
(half-angle = 7 deg)	(radius = 15.9 mm)	(AR = 1.5, half-angle = 24 deg)	(+50.8 mm)
——	——	Converging	Downstream
		(AR = 0.5, half-angle = 12 deg)	(−50.8 mm)

[a]AR = area ratio of nozzle.

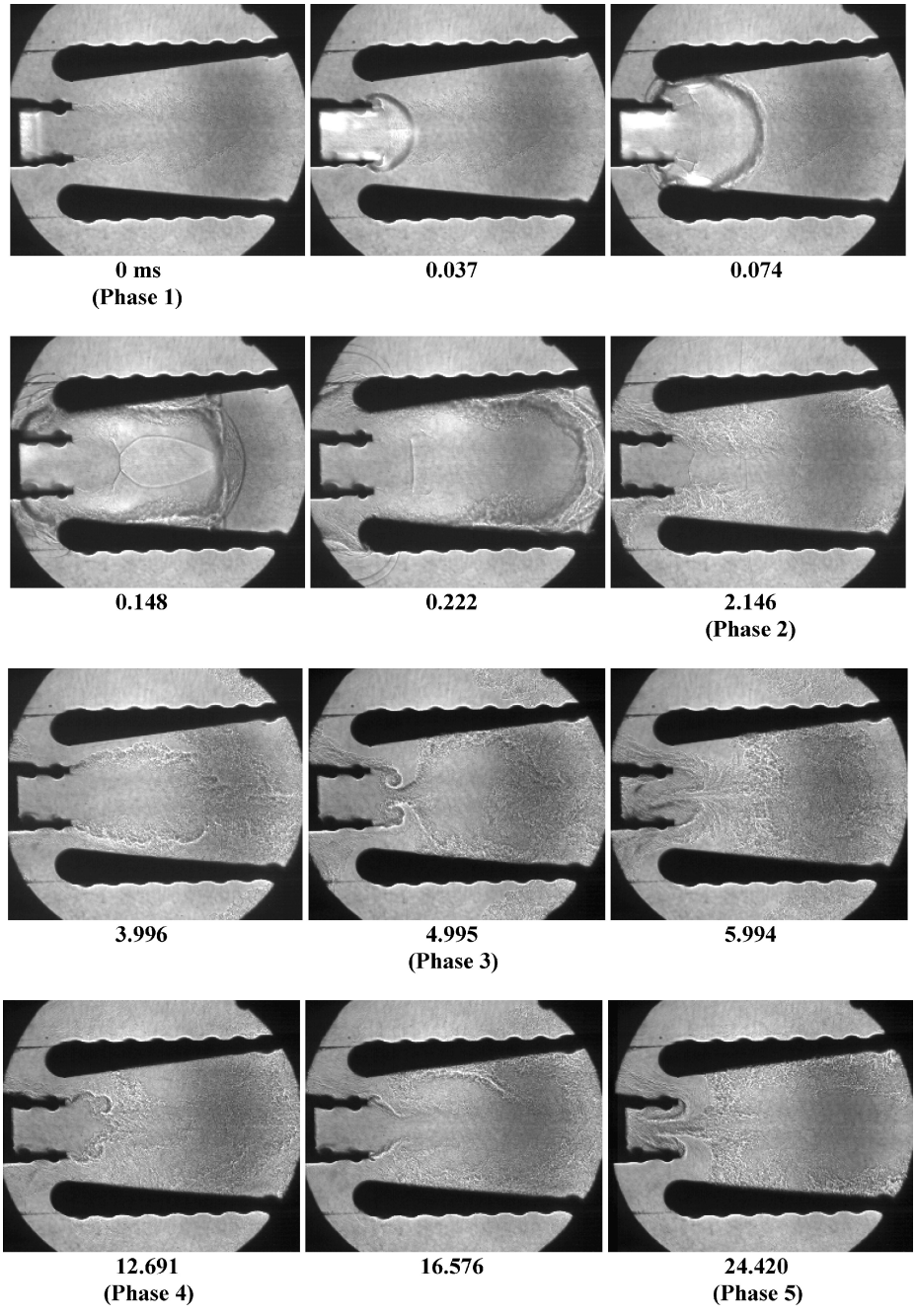

Fig. 3 Shadowgraph time series of a PDE with a diverging ejector.

constraints of the acrylic glass, it was only possible to run the PDE for approximately 1 s (or 10 PDE cycles). However, the shadowgraph visualizations were compared for the various cycles within this time frame. It was determined that there were no visible cycle-to-cycle variations that needed to be accounted for.

Results and Discussion

PDE Ejector Cycle

Analysis of the high-speed shadowgraph images in conjunction with detonation-tube pressure data revealed that the PDE–ejector cycle could be decomposed into five basic temporal phases: 1) exiting of the detonation wave from the PDE followed by an initial flow reversal out of the ejector inlet, 2) generation of positive entrainment into the ejector inlet, 3) a first stage of overexpansion of the PDE resulting in the fluid flowing back into the PDE tube, 4) steady entrainment accompanied by strong flow and pressure oscillations, and 5) a second and much stronger stage of flow reversal inside the detonation tube. These five parts of the PDE–ejector cycle are depicted in the pressure–time trace and series of shadowgraph images given in Figs. 2 and 3, respectively. Each image in the shadowgraph sequence of Fig. 3 is labeled with the corresponding time in milliseconds relative to the time of exit of the detonation wave. The approximate start of each "phase" is also indicated below the appropriate images. In all the shadowgraph images presented in this paper, the ejector and nozzle surfaces appear to be wavy. This waviness is not physical, but rather the surfaces of the ejectors and

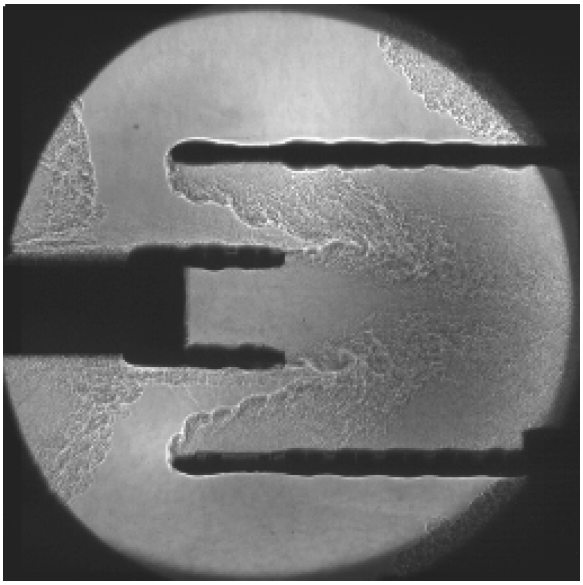

a)

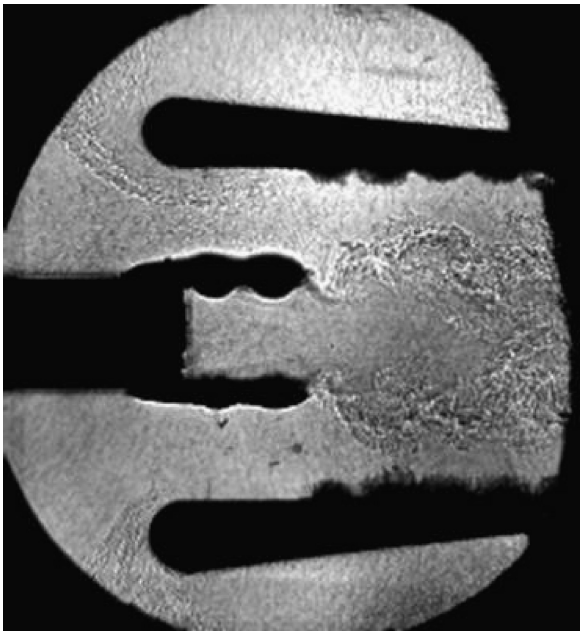

b)

Fig. 4 Effect of ejector inlet geometry on secondary flow entrainment ($t = 3.2$ ms): a) sharp-edged ejector inlet and b) contoured ejector inlet.

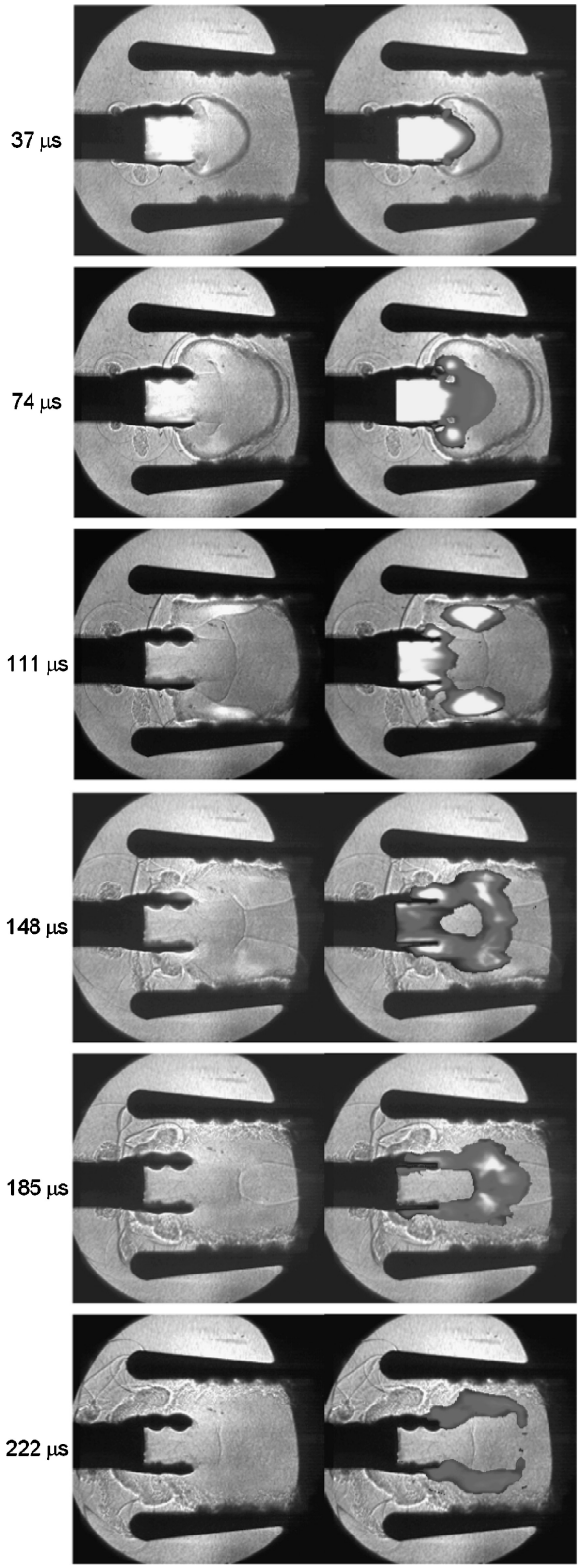

Fig. 5 Correlation between shadowgraphs and visible flame luminosity.

nozzles exposed to the flow are smooth. The apparent waviness is a result of the diffraction of light by the exterior bolts holding the ejector and nozzle hardware in place and is due to changes in index of rarefaction of the acrylic sheets due to stresses the bolts produced.

The high-speed images shown in Fig. 3 reveal that the high-pressure gases following the detonation wave initially wrapped around the exhaust nozzle of the PDE and produced negative entrainment during a very short time period of approximately 1.0 ms. Following this transient expulsion of primary gas, the ejector began entraining the expelled gas in addition to ambient secondary flow. This strong entrainment is visible during the remainder of the blow-down portion of the PDE cycle. The blowdown portion of the cycle was defined as the duration for which the PDE pressure initially remained above atmospheric pressure after a detonation event. This duration was seen to be approximately 4.8 ms, as shown in Fig. 3. Thus, for this particular PDE–ejector system of a straight nozzle and diverging ejector, positive entrainment was observed during 79% of the cycle. After the blowdown portion of the cycle, the PDE–ejector overexpanded to subatmospheric pressures, as was seen in the pressure–time trace of Fig. 2. The overexpansion was also indicated by flow reversal back into the PDE in the shadowgraph images of Fig. 3 (see $t = 4.995$ ms). Following this first flow reversal (phase 3), positive flow rate was observed exiting from the PDE exhaust as depicted in the $t = 12.691$ ms image of Fig. 3. The exhaust flow was then observed to oscillate, forming strong vortices, until the PDE underwent another strong overexpansion and resulted in a second stage of flow reversal as shown by the $t = 24.420$ ms image of Fig. 3. The second stage of flow reversal was observed in the shadowgraph visualizations to be much greater in strength and duration than the first flow reversal. Although the PDE–ejector cycle for almost every configuration tested could be decomposed into these five basic phases, the details of each phase were observed to be affected by the shape of the ejector inlet geometry, the PDE exhaust nozzle, and the axial placement of the ejector relative to the exhaust plane of the PDE. These three important geometrical parameters are addressed next.

Ejector Inlet Geometry

The first parameter investigated in this study was the inlet shape of an ejector with a straight (constant-area) internal cross section. Figure 4 shows a pair of shadowgraph images for the cases of an ejector augmenter without and with a contoured ejector inlet installed. Due to geometrical limitations of contouring the ejector inlet, the exterior surface of the ejector shown in Fig. 4b was tapered to converge back to the constant interior diameter of the ejector. Without the contoured inlet, severe flow separation of the entrained gases was observed at the sharp leading edge of the ejector plates. However, by rounding the inlet of the ejector, this flow separation was prevented and the time at which positive entrainment was observed occurred 0.3 ms sooner in the PDE–ejector cycle. Furthermore, the contoured ejector inlet was observed to generate a greater amount and longer duration of mass flow entrainment than that of the sharp-edged ejector. This increased efficiency in mass entrainment would translate into greater thrust augmentation in a practical application.

The coupling between the shock/flow structures and the flame was visualized by turning off the shadowgraph light source and imaging only the broadband visible luminosity from the flame. A false red-yellow coloring palette was used to enhance the visualization of the original grayscale luminosity images, with yellow being the brightest and red the darkest. The resulting flame luminosity images were then superimposed onto the shadowgraph images as shown in Fig. 5 for the straight (constant-area) nozzle and contoured ejector configuration. This sequence shows that the flame began to decouple from behind a quasi-spherically expanding shock wave 37 μs after the nearly planar detonation wave had entered the viewing area. The underexpanded PDE exhaust jet developed expansion waves along the periphery of the PDE exhaust nozzle, causing local quenching of the flame (74 μs time frame). As the flow continued to expand, the level of flame quenching extended to the core of the jet, but flame holding appears to have occurred on the exterior walls of the exhaust nozzle due to a recirculating vortex.

Figure 5 also shows that at 111 μs flame luminosity appeared as the decoupling leading shock wave collided with the interior wall of the straight ejector. The presence of flame luminosity in this region signifies an increase in heat release due to the shock compression near the ejector wall. The following Mach reflection of the leading shock wave, observed at 148 and 185 μs, caused the immediate trailing gases to experience an increase in pressure. The compression produced by these shock waves resulted in increased burning rates, as visualized by the increased luminosity along the shock waves. However, the large expansion cell formed directly at the exit of the PDE nozzle still produced local flame quenching for these times.

PDE Exhaust Nozzle Geometry

The global structure of the PDE–ejector blowdown cycle did not change much with the nozzle geometry of the PDE (Fig. 6), but some details of the process that did vary could contribute to a change in thrust augmentation. First, the structure of the exiting detonation shock wave was altered by the nozzle geometry, as seen at time 0.074 ms. Although the exiting shock waves from the straight and diverging nozzles were both observed to have flat profiles near the axis of the PDE tube, the converging nozzle produced a more axially focused shock wave. This was a result of the shock being accelerated

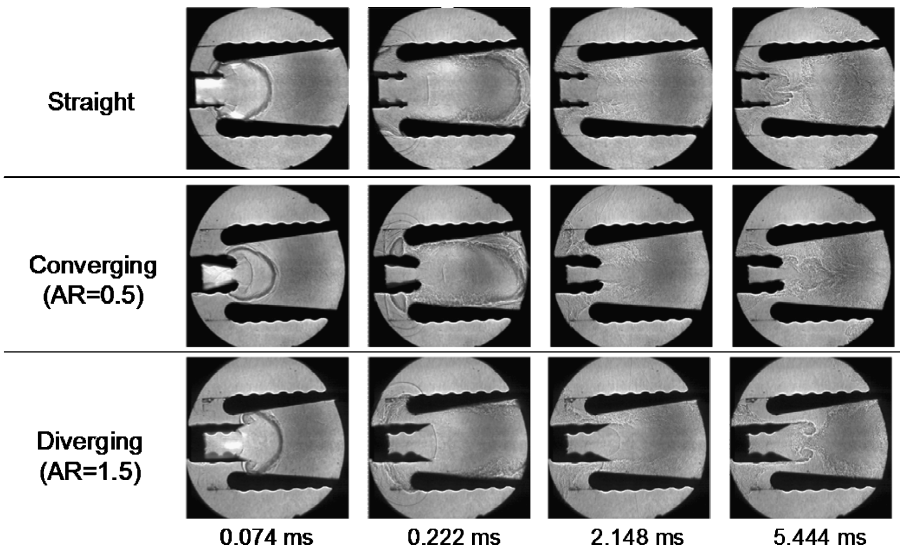

Fig. 6 Shadowgraphs for three PDE nozzle geometries with a diverging ejector.

by the area reduction of the converging nozzle. Also, the leading Mach disk was observed (0.222 ms) to be located closer to the exit plane of the PDE exhaust nozzle as the area ratio (AR) of the nozzle was increased. This signified that the flow at this time was more perfectly expanded with a diverging nozzle (AR = 1.5) compared to the straight (AR = 1) and converging nozzles (AR = 0.5). All three nozzles produced similar positive levels of entrainment for the majority of the PDE cycle.

Two periods of detonation tube flow reversal were observed in the high-speed shadowgraph visualizations as a result of the PDE overexpanding below atmospheric pressure. For the straight nozzle configuration, the first period of flow reversal began at an approximate time of 5.4 ms after the detonation wave exited from the PDE as shown in Fig. 7, whereas the second stage of flow reversal was observed at 25 ms. The behavior of flow reversal for the diverging nozzle configuration was observed to be very similar to that of the straight nozzle. However, the first stage of flow reversal immediately after the blowdown process was not observed for the converging nozzle. The absence of a first stage of flow reversal with the converging nozzle was due to the nozzle area reduction not allowing the pressure in the tube to overexpand. However, the flow was allowed to overexpand later in the cycle (~28.4 ms) with the converging nozzle. The second stage of flow reversal for the converging nozzle occurred at a much later time compared to the straight and diverging nozzle configurations due to the associated increase in PDE blowdown time. Through the use of the shadowgraph visualizations, it was concluded that all configurations tested clearly showed a stronger level of flow reversal during the second stage. This observation is consistent with the pressure trace provided in Fig. 2.

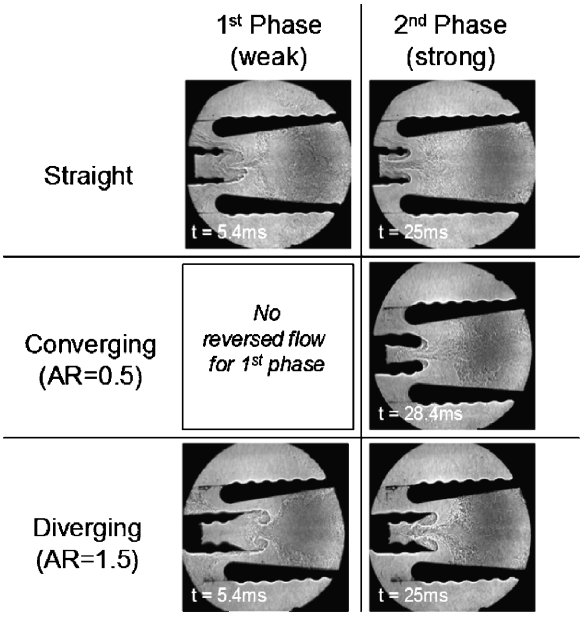

Fig. 7 Effect of nozzle geometry on PDE tube flow reversal.

By tracking the features in the flow using cross-correlation algorithms, a pseudovelocity vector map was obtained. This technique has been referred to as CSV.[11] The vectors qualitatively represent the direction and magnitude of the propagation of the coherent flow structures (density gradients in this case) and correspond well with the observations made from the shadowgraph visualizations. Sample vector plots for the first stage of flow reversal for the straight nozzle and diverging ejector configuration are given in Fig. 8. Prior to the complete reversed flow, positive secondary flow entrainment was observed to enter the ejector inlet and collide in a stagnation region downstream of the PDE exhaust nozzle. The first vector plot corresponds to this state in the detonation cycle (2.444 ms). The stagnation point was observed to move upstream as the PDE tube overexpanded below atmospheric pressure and eventually resulted in reversed flow back into the PDE tube. The vector plot corresponding to 5.444 ms shows the flow reversal back into the detonation tube.

Axial Position of Ejector

The axial placement of the ejector relative to the PDE nozzle exit can also affect the mass entrainment. The diverging nozzle and diverging ejector configuration were selected for studying this parameter. Figure 9 shows that a 2-in. (50.8-mm) downstream placement of the ejector resulted in the impingement of the detonation wave on the ejector inlet walls. This impingement would contribute to a negative thrust production during this portion of the cycle. However, placing the ejector upstream would produce a positive thrust production because the exiting detonation wave collided on the internal thrust bearing surface of the diverging cross-sectional area ejector as shown in Fig. 9.

The dynamics of the flow entrainment was also observed to be affected by the ejector's axial placement, as shown in the set of images in Fig. 9 corresponding to the time of 5.444 ms. For example, during this first stage of PDE tube flow reversal, the initial location of the stagnation point appeared to form farther downstream from the PDE exhaust nozzle as the ejector was moved upstream. This was

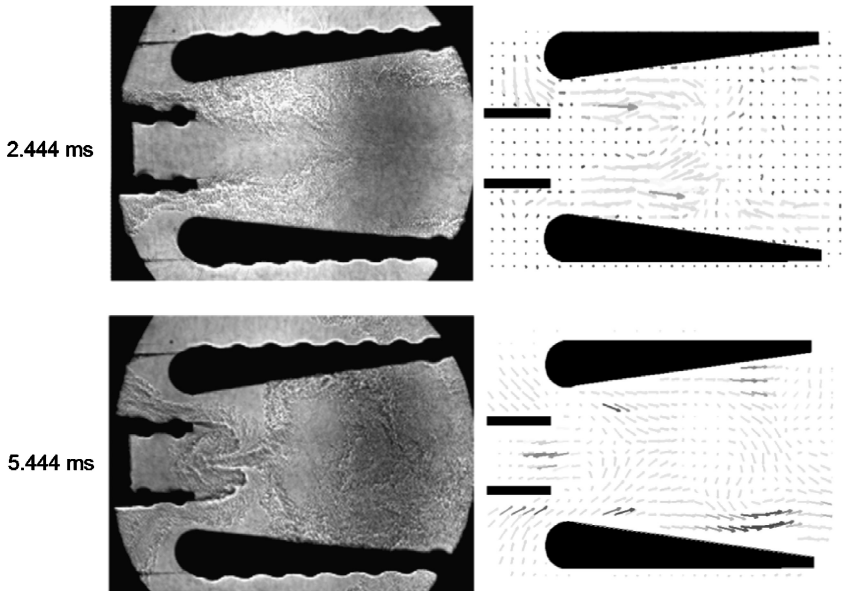

Fig. 8 CSV vectors for the first stage of the straight nozzle PDE tube flow reversal.

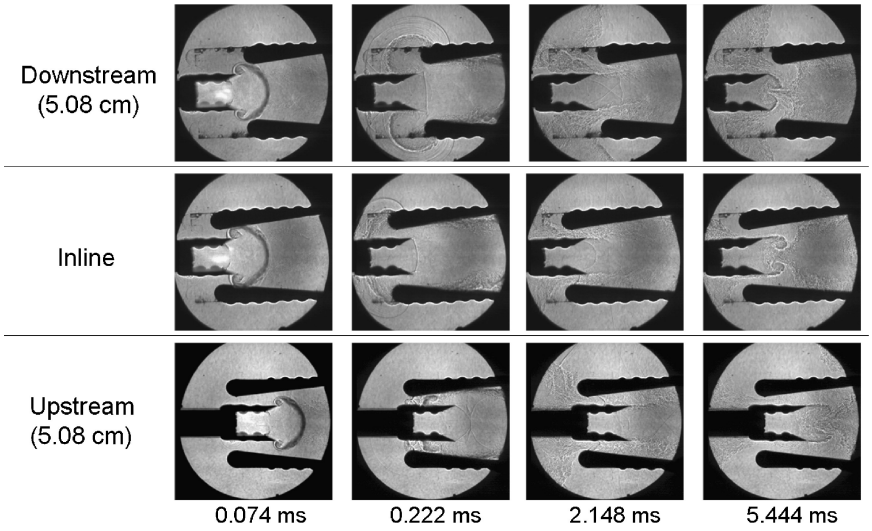

Fig. 9 Shadowgraphs showing the effects of ejector axial placement.

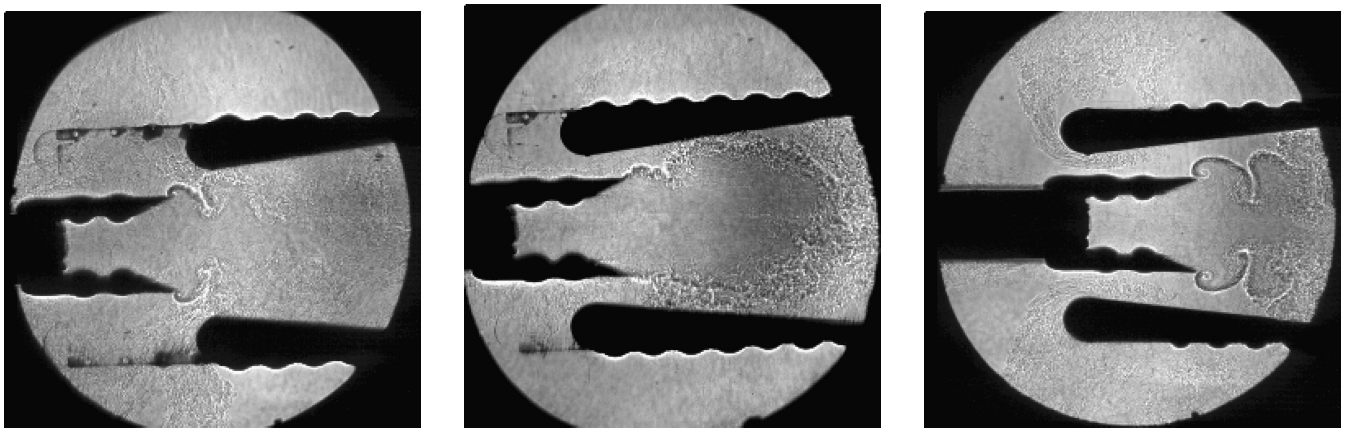

Fig. 10 Flow oscillations observed in PDE exhaust flow for a) upstream, b) inline, and c) downstream axial placements ($t \sim 15$ ms).

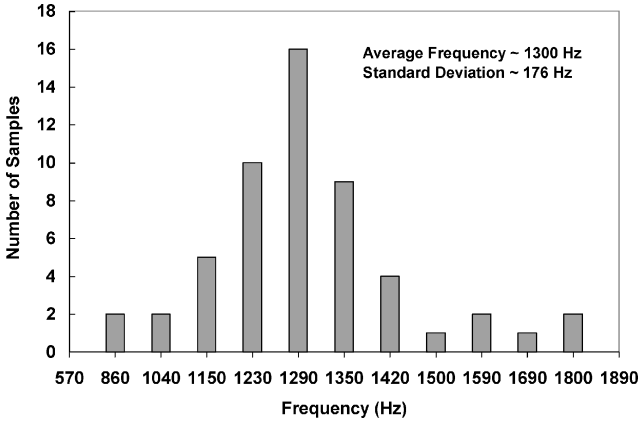

Fig. 11 Computed frequency of flow oscillations for tested conditions.

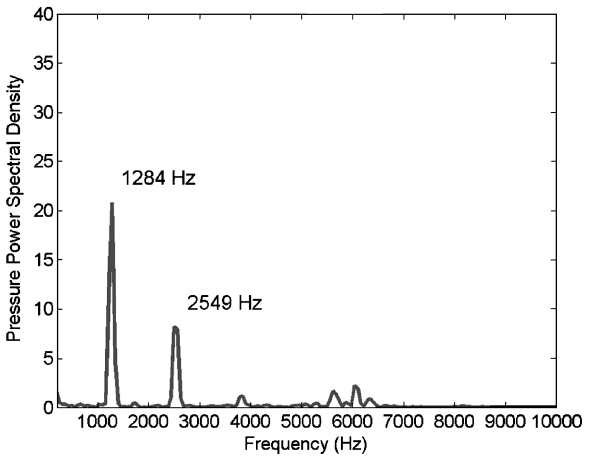

Fig. 12 Spectrum analysis of PDE pressure measurements.

probably due to the increased flow turning required by the flow when placing the ejector upstream. With a 50.8-mm downstream placement, the entrained flow had a direct path into the PDE exhaust nozzle. However, the 50.8-mm upstream placement required the flow to perform a much more demanding 180-deg turning of the flow. Thus, a slight downstream axial placement of the ejector appeared to provide the least resistance to secondary mass flow entrainment. This observation is consistent with the performance data provided by Rasheed et al.[6] for a straight axisymmetric PDE–ejector configuration. Their data showed enhanced thrust augmentation with a slight downstream placement of the ejector.

An additional observation made during the axial ejector placement studies was the interaction of the dynamic shear-layer instabilities with the flow entrainment. During the time between the two flow reversal stages, large-scale coherent vortices were formed in the exhaust shear layer as shown in Fig. 10 for the diverging nozzle and diverging ejector configuration. These vortices produced an alternating positive/negative entrainment for the downstream-placed ejector. As the large-scale vortices formed in the initial shear layer, they pushed the secondary flow out of the ejector inlet, resulting in

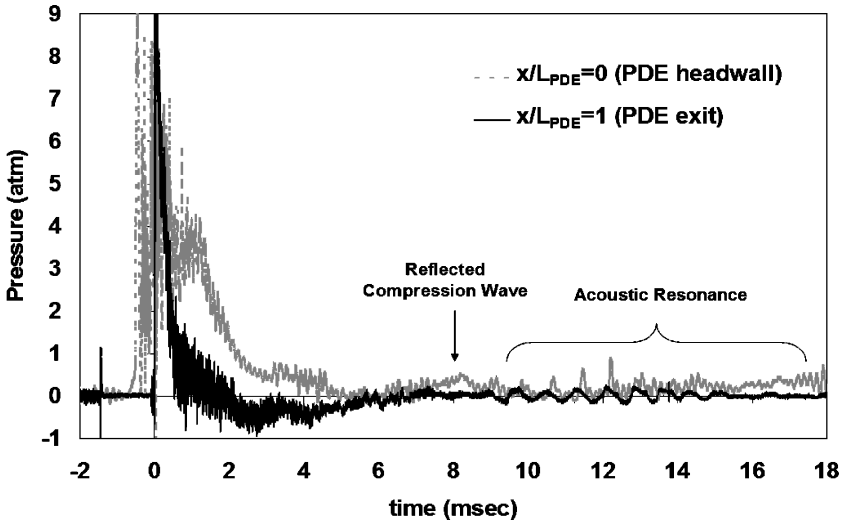

Fig. 13 Correlation between PDE headwall and exit gauge pressure.

negative flow entrainment. Then, as the vortices convected downstream, the ejector positively entrained flow again. By moving the ejector upstream, this interaction between the ejector inlet flow and the shear-layer vortices was decoupled. Positive entrainment was observed for both the inline and upstream-placed ejectors during this portion of the cycle.

The formation of strong vortices or flow oscillations during the time period between the flow reversal stages was observed not only for the diverging geometries but also for most of the other tested hardware as well. The frequency of formation of the vortices was nearly consistent for all reported cases, but the strength or coherence of these vortices was affected by the ejector and/or nozzle geometry. The average frequency of the vortices was measured from all the high-speed shadowgraph visualizations to be approximately 1300 Hz with a standard deviation of about 180 Hz. Figure 11 shows the distribution of the measured vortex shedding frequencies.

The source of excitation of these strong vortices is believed to be from an acoustic resonance of the detonation tube. The detonation tube pressure trace given previously in Fig. 2 shows the presence of cyclic pressure oscillations during this same stage of the PDE–ejector cycle. Presented in Fig. 12 is a Fourier analysis of the pressure data, which reveals a fundamental resonance at 1284 Hz along with a near second harmonic at 2549 Hz. This fundamental frequency of 1284 Hz correlates well with the observed 1300-Hz frequency in the exhaust flow oscillations. From the associated length scales of this high frequency, the possibility of a Helmholtz or quarter-wave mode of the detonation tube was eliminated. Pressure data recorded at the headwall and end of the detonation tube are plotted in Fig. 13 and show the resonant behavior to initiate first in time at the headwall of the tube after an upstream-propagating compression wave collided with the headwall. This reflected compression wave is believed to have excited a half-wave standing acoustic mode between the headwall of the detonation tube and the first DDT obstacle (blockage ratio = 0.5) located 0.171 m downstream. The amplitude of pressure oscillations was observed to be much stronger near the headwall of the tube, causing perturbations to the incoming PDE airstream, which resulted in a pulsing exhaust flow at the frequency of 1300 Hz.

Conclusions

A parametric study of a two-dimensional ejector integrated with a PDE was performed. High-speed shadowgraphy was used to visualize the flow inside the ejector. Correlations between the observed shock/flow structures and the sooty, high-heat-release regions of the exhaust flow were obtained through synchronized shadowgraph and flame luminosity imaging. The flame was observed to initially decouple from the quasi-spherical expanding shock wave but reignition occurred as the leading shock waves collided and reflected off of the interior walls of the ejector. Later in the cycle, quenching of the flame was seen to occur in the first expansion cell of the exhaust jet, followed by reignition due to the strong Mach disk structure in the jet core.

Several geometrical parameters were found to be important in the PDE–ejector's performance. A rounded ejector inlet was observed to produce significantly more entrainment than an ejector with a sharp-edged inlet. The sharp-edged ejector inlet experienced severe flow separation and very little mass entrainment.

The exhaust nozzle geometry was varied from an AR of 0.5 to 1.5. All three nozzles produced similar positive levels of entrainment for the majority of the PDE cycle. However, some details of the process did vary, which could contribute to a change in the thrust augmentation. For example, the converging nozzle (AR = 0.5) produced the most underexpanded jet during the blowdown process based on the observed shock structures. This translated into higher pressures inside the PDE chamber for a longer duration, signifying possible thrust benefits of using a converging nozzle. Also, the converging nozzle prevented overexpansion (flow reversal) of the detonation tube early in the cycle.

The CSV technique was used to visualize the first flow reversal stage of the straight nozzle configuration. The vectors clearly showed how the entrained flow entered the ejector, mixed with the primary flow, and collided in a downstream stagnation region. As the tube overexpanded, the stagnation point was pulled inside the detonation tube, resulting in complete flow reversal. This is the first reported application of this technique to PDE–ejector flows and was successful due to the strong density gradients and the high framing rate of the camera.

The final parameter varied was the axial position of the ejector relative to the exit of the PDE. During the initial portion of the detonation cycle, the axial position of the ejector altered the location of impingement of the exiting detonation wave. With a downstream placement, this shock impingement could produce a short time of negative thrust augmentation. The level of PDE tube flow reversal was also observed to be changed by the axial placement. Later in the PDE cycle, a coupling between ejector mass entrainment and large-scale vortices shed ($\sim$1300 Hz) in the exhaust jet shear layer was seen to occur when the ejector was placed downstream of the PDE. An alternating positive/negative entrainment was generated by the vortex–inlet coupling.

Acknowledgments

The University of Cincinnati authors thank the financial support provided by the NASA Glenn Research Center under Grant NAG3-2669 and the technical support of Terry Meyer of Innovative Scientific Solutions, Inc., on the coherent structure velocimetry calculation technique. The assistance provided by Eric Cornell during experimental testing is greatly appreciated.

References

[1]Porter, J. L., and Squyers, R. A., "A Summary/Overview of Ejector Augmentor Theory and Performance," Vought Corp. Advanced Technology Center, ATC Rept. R-91100/CR-47A, Dallas, TX, 1979.

[2]Paxson, D. E., Wilson, J., and Dougherty, K. T., "Unsteady Ejector Performance: An Experimental Investigation Using a Pulsejet Driver," AIAA Paper 2002-3915, July 2002.

[3]Wilson, J., and Dougherty, K. T., "Unsteady Ejector Performance: An Experimental Investigation Using a Resonance Tube Driver," AIAA Paper 2002-3632, July 2002.

[4]Johnson, W. S., and Yang, T., "A Mathematical Model for the Prediction of the Induced Flow in a Pulsejet Ejector with Experimental Verification," American Society of Mechanical Engineers, Paper 68-WA/FE-33, 1968.

[5]Hoke, J., Bradley, R., Stutred, J., and Schauer, F., "Integration of a Pulsed Detonation Engine with an Ejector Pump and with a Turbo-Charger as Methods to Self-Aspirate," AIAA Paper 2002-0615, Jan. 2002.

[6]Rasheed, A., Tangirala, V., Pinard, P. F., and Dean, A. J., "Experimental and Numerical Investigations of Ejectors for PDE Applications," AIAA Paper 2003-4971, July 2003.

[7]Shehadeh, R., Saretto, S., Lee, S.-Y., Pal, S., and Santoro, R. J., "Experimental Study of a Pulse Detonation Engine Driven Ejector," AIAA Paper 2003-4972, July 2003.

[8]Allgood, D., Gutmark, E., and Katta, V., "Effects of Exit Geometry on the Performance of a Pulse Detonation Engine," AIAA Paper 2002-0613, Jan. 2002.

[9]Yungster, S., and Perkins, H. D., "Multiple Cycle Simulation of a Pulse Detonation Engine Ejector," AIAA Paper 2002-3630, July 2002.

[10]Groschel, E., Tsuei, H., Xia, G., and Merkle, C., "Characterization of Thrust Augmentation by Unsteady Ejectors," AIAA Paper 2003-4970, July 2003.

[11]Meyer, T., Brown, M., Fonov, S., Goss, L., Gord, J., Shouse, D., Belovich, V., Roquemore, W., Cooper, C., Kim, E., and Haynes, J., "Optical Diagnostics and Numerical Characterization of a Trapped-Vortex Combustor," AIAA Paper 2002-3863, July 2002.

M. Sichel
Associate Editor